IEEE Access
Multidisciplinary | Rapid Review | Open Access Journal

SPECIAL SECTION ON MISSION CRITICAL SENSORS AND SENSOR NETWORKS (MC-SSN)

Received April 11, 2018, accepted May 17, 2018, date of publication May 22, 2018, date of current version June 19, 2018.

Digital Object Identifier 10.1109/ACCESS.2018.2839690

UWB Radar Target Detection Based on Hidden Markov Models

GANLIN ZHAO[1], QILIAN LIANG[1], (Fellow, IEEE), AND TARIQ S. DURRANI[2], (Fellow, IEEE)
[1]Department of Electrical Engineering, University of Texas at Arlington, Arlington, TX 76019-0016, USA
[2]Department of Electronic and Electrical Engineering, University of Strathclyde, Glasgow G1 1XQ, U.K.

Corresponding author: Ganlin Zhao (ganlin.zhao@mavs.uta.edu)

This work was supported in part by NSFC under Grant 61731006, Grant 61771342, Grant 61711530132, in part by the Royal Society of Edinburgh, and in part by the Tianjin Higher Education Creative Team Funds Program.

ABSTRACT In this paper, we propose ultra-wideband (UWB) radar target detection approach based on Hidden Markov Models (HMMs). HMMs are used as a classifier to identify signal with the presence of target in a background clutter and the pure clutter response signal. Time-frequency features are extracted and features have less correlation to each other are selected based on the feature covariance matrix and fed into HMMs. The detection experiments are conducted in two different scenarios: sense-through-foliage target detection and sense-through-wall human detection. The sense-through-foliage data set contains poor quality UWB radar return echoes using low amplitude transmitting pulses. Data collected from different radar locations are tested and detection results are presented. Sense-through-wall data are collected using different UWB radar and the target is human standing behind different types of walls. HMMs parameters are also investigated to optimally model UWB radar signals for target detection.

INDEX TERMS Target detection, UWB, HMM, sense-through-foliage, sense-through-wall.

I. INTRODUCTION

Radar target detection is an important technique in remote sensing research and homeland security applications. The returned echoes from unwanted objects (known as clutter) such as ground, sea, trees, buildings and atmospheric turbulences can often make the real target fade into the environment and complicate the detection task. For example, clutter echoes may contain more power than target echoes and threshold based detection methods may result in high false alarm rate. In practical situations, warfighters on the battleground are always facing unknown indirect enemy threats from covers. Law enforcement and rescue missions are confronted with situations to identify life signals behind walls and ruins. Therefore, increasing target detection accuracy is of great importance for these applications.

In this work, we deal with both sense-through-foliage and sense-through-wall target detection problems. Considering the non-stationary nature of foliage environment, doppler spread induced by clutter motion and multi-path clutter backscattering can degrade detection performance. We further consider a more challenging situation that data collected from radar sensors are not perfect, for example, poor quality echo signal. Sense-through-wall human detection relies on capturing doppler shift caused by micro motion (e.g. human breath and chest movement) [1]. However, irregular contours of human bodies make themselves not perfect radar signal reflectors. Return signals of ideal reflectors (e.g. metallic objects) usually have dominant path.

UWB radar is characterized by a large instantaneous fractional energy bandwidth and waveforms formed by pulses with very short duration [2]. Good penetration ability and high range resolution make UWB radar a good candidate for target detection behind clutter.

Hidden Markov model (HMM) is an example of dynamic bayesian network. It statistically models temporal data and especially has success in speech recognition [3], [4], text classification [5], [6], machine translation [7] and other pattern recognition applications [8]–[10]. Recently, Hidden Markov Model based methods have been applied to variant pattern recognition problems including radar target detection, classification and tracking problems since radar signal is essentially temporal. Hidden Markov Model models a stochastic process with a sequence of observations produced by underlying unobserved states transitions. The states are ''Hidden'' and follow a Markov process. Compared to deterministic model, Hidden Markov Model has rich mathematical foundation and models the signal as a parametric random process. The parameters of such random process can be precisely

2169-3536 © 2018 IEEE. Translations and content mining are permitted for academic research only.
Personal use is also permitted, but republication/redistribution requires IEEE permission.
See http://www.ieee.org/publications_standards/publications/rights/index.html for more information.

estimated using well-defined algorithms. In this paper, we propose to use Hidden Markov Model based method for UWB radar target detection by constructing HMMs for target and non-target cases. The results presented by this paper provide validation and performance evaluation of using such method for radar target detection. The testing data are real world collection of UWB radar echoes. Furthermore, we study optimal model parameters to distinguish between target and non-target signal models in terms of probability of detection and false alarm rate.

The rest of this paper is organized as follows: In Section II, we introduce the background knowledge of Hidden Markov Models. In Section III, we propose the HMM based target detection approach. In Section IV, we describe sense-through-foliage and sense-through-wall data sets. In Section V, we provide experiment results obtained by two sets of UWB testing data. In Section VI, we draw the conclusion.

II. INTRODUCTION TO HIDDEN MARKOV MODELS

Hidden Markov Model was firstly introduced in the late 1960s and have gained increasing popularity for a wide range of applications. By characterizing the statistical properties of the signal model, HMMs can be used to model both stationary and non-stationary random process. Generally, an HMM consists of two random processes. The first process is on time dimension which is essentially a first order Markov chain and at each time t ($t \in \{1, T\}$) the system is in state q_t with N possible finite states choices:

$$S = \{S_1, S_2, \ldots, S_N\} \tag{1}$$

In the second random process, each state produces an observation result which is directly visible. However, the states are "Hidden" and not observable. In other word, we cannot directly tell the exact state where the observation occurs. The T observation symbols are

$$O = \{O_1, O_2, \ldots, O_T\} \tag{2}$$

A basic HMM is characterized by three sets of parameters, we use v_t to represent the observation symbol at time t:

1) Initial state probability matrix $\pi = \{\pi_i\}$, where each element $\pi_i = P(q_1 = S_i)$, $1 \le i \le N$ is the probability that the system is in state i at initial time $t = 1$.
2) State transition probability matrix $A = \{a_{ij}\}$, where $a_{ij} = P(q_t = S_j \mid q_{t-1} = S_i)$, $1 \le i, j \le N$ is the probability that the system is in state j at time t given that the system is in state i at time $t - 1$.
3) Observation probability matrix $B = \{b_j(t)\}$, where $b_j(t) = P(v_t = O_t \mid q_t = S_j)$, $1 \le j \le N, 1 \le t \le T$ is the probability that the output observation symbol is O_t given the system is in state j at time t.

The notation $\lambda = \{A, B, \pi\}$ denotes a complete parameter set of HMM. In addition, if the observation symbol probability density function is discrete, an HMM is called discrete Hidden Markov Model. Otherwise, it is called continuous Hidden Markov Model. For continuous case, the states transition probability density functions are typically represented as a form of Gaussian mixtures [11]–[14].

HMM has been proven useful to solve real world problems, which can be emphasized into three basic categories [3]:

1) Evaluation. Compute the probability of an observation sequence $P(O \mid \lambda)$ given a model $\lambda = (A, B, \pi)$. One possible solution for calculating $P(O \mid \lambda)$ is by summing the joint distribution $P(O, Q \mid \lambda)$ over every possible state sequences based on Bayesian method,

$$\begin{aligned} P(O \mid \lambda) &= \sum_{Q} P(O, Q \mid \lambda) P(Q \mid \lambda) \\ &= \prod_{t=1}^{T} P(O_t \mid q_t, \lambda) \prod_{t=1}^{T} P(q_t \mid q_{t-1}, \lambda) \\ &= \sum_{q_1, q_2, \ldots q_T} \pi_{q_1} b_{q_1}(O_1) a_{q_1 q_2} b_{q_2}(O_2) \ldots \\ &\quad \ldots a_{q_{T-1} q_T} b_{q_T}(O_T) \end{aligned} \tag{3}$$

This brute force computing method involves the order of $2TN^T$ calculations which is not practical to satisfy real application demand [15]. Fortunately, an alternative approach called forward algorithm can efficiently compute $P(O \mid \lambda)$ with much lower complexity of $O(N^2 T)$. Define forward probability $\alpha_t(j)$ as the probability of being in state j after observing first t partial observation symbols $O_1, O_2, \ldots O_t$:

$$\alpha_t(j) = P(O_1, O_2, \ldots O_t, q_t = S_j \mid \lambda) \tag{4}$$

$\alpha_t(j)$ can be solved inductively in three steps:

a) Initialization:

$$\alpha_1(j) = \pi_j b_j(O_1) \quad 1 \le j \le N \tag{5}$$

b) Recursion:

$$\alpha_t(j) = \sum_{i=1}^{N} \alpha_{t-1}(i) a_{ij} b_j(O_t) \qquad 1 \le j \le N, 1 \le t \le T \tag{6}$$

c) Termination:

$$P(O \mid \lambda) = \sum_{i=1}^{N} \alpha_T(i) \tag{7}$$

2) Decoding. Find an optimal hidden state sequence S associated with an observation sequence O given a model $\lambda = (A, B, \pi)$. There are several criteria to define the "optimal" sequence. The most widely used criteria is to find the state sequence that maximize $P(Q, O \mid \lambda)$ by employing the Viterbi Algorithm [16].
3) Learning. Estimate model parameters $\lambda = (A, B, \pi)$ to maximize the probability of given observation sequence $P(O \mid \lambda)$. To find the optimal parameters of the HMM associated with the observation sequence is

difficult and there is no way to analytically find the optimal estimation. However, $P(O \mid \lambda)$ can be locally maximized using the Baum-Welch algorithm [17] [18] to efficiently find the maximum likelihood estimation of model parameters. Baum-Welch algorithm is essentially a special case of the Expectation-Maximization algorithm using iterative estimation approach given an initial guess of the probabilities. In each iteration a better estimation is computed to guarantee that $P(O \mid \hat{\lambda}) > P(O \mid \lambda)$ until the algorithm converges. To describe the Baum-Welch algorithm, we firstly need to define a backward probability $\beta_t(i)$ as the probability of given the system being in state j at time t after observing partial observation symbols $O_{t+1}, O_{t+2}, \ldots O_T$ from $t+1$ to the end:

$$\beta_t(i) = P(O_{t+1}, O_{t+2}, \ldots O_T \mid q_t = S_i, \lambda) \tag{8}$$

Similar to the forward probability, $\beta_t(i)$ can also be computed inductively:

a) Initialization:

$$\beta_T(i) = 1 \quad 1 \le i \le N \tag{9}$$

b) Recursion:

$$\beta_t(i) = \sum_{j=1}^{N} a_{ij} b_j(O_{t+1}) \beta_{t+1}(j) \quad 1 \le i \le N, 1 \le t \le T \tag{10}$$

Before estimation of parameter A and B, a probability $\xi_t(i,j)$ is defined as the probability of being in state i at time t and state j at time $t+1$, given the observation and the model:

$$\xi_t(i,j) = P(q_t = S_i, q_{t+1} = S_j \mid O, \lambda) \tag{11}$$

and can be computed using forward and backward probabilities as:

$$\xi_t(i,j) = \frac{P(q_t = S_i, q_{t+1} = S_j, O \mid \lambda)}{P(O \mid \lambda)} \tag{12}$$

$$= \frac{\alpha_t(i) a_{ij} b_j(O_{t+1}) \beta_{t+1}(j)}{\sum_{i=1}^{N} \sum_{j=1}^{N} \alpha_t(i) a_{ij} b_j(O_{t+1}) \beta_{t+1}(j)} \tag{13}$$

Another probability $\gamma_t(j)$ is also defined as the probability of being in state S_j at time t given the observation and model:

$$\gamma_t(j) = P(q_t = S_j \mid O, \lambda) \tag{14}$$

which can be computed as

$$\gamma_t(j) = \frac{P(q_t = S_j, O \mid \lambda)}{P(O \mid \lambda)} \tag{15}$$

$$= \frac{\alpha_t(j) \beta_t(j)}{\sum_{j=1}^{N} \alpha_t(j) \beta_t(j)} \tag{16}$$

The EM algorithm can be used to reestimate the model parameter A and B after initialization. Each iteration can be divided in to E-step (Expectation) and M-step (Maximization):

E-Step:

1) Recursively compute $\alpha_t(j)$ and $\beta_t(j)$
2) Compute $\xi_t(i,j)$ and $\gamma_t(j)$

M-Step: Reestimate a_{ij} and b_{ij}

1)

$$\hat{a}_{ij} = \frac{\sum_{t=1}^{T-1} \xi_t(i,j)}{\sum_{t=1}^{T-1} \sum_{k=1}^{N} \xi_t(i,k)} \tag{17}$$

2)

$$\hat{b}_j(v_k) = \frac{\sum_{t=1, s.t. O_t = v_k}^{T} \gamma_t(j)}{\sum_{t=1}^{T} \gamma_t(j)} \tag{18}$$

III. HIDDEN MARKOV MODEL BASED UWB RADAR TARGET DETECTION

In our work, our task is to detect target in background clutter using UWB radar echoes. To tackle with this problem using Hidden Markov Model based method, Baum-Welch algorithm is firstly used to train different HMMs for both target and no target respectively. Then the testing sequences can be fed into each HMM to obtain a likelihood for each model. The decision of whether target is present or not is based on which model the testing sequence scores a higher likelihood. The detection method is shown in Figure 1.

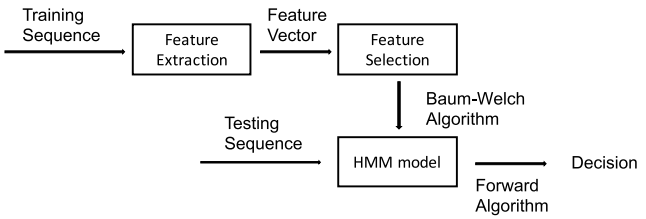

FIGURE 1. Block diagram of HMM based target detection.

A. FEATURE EXTRACTION AND SELECTION

To provide effective input sequences for HMM training, we need to extract features that can well represent the target signature. Firstly, received radar signal is evenly divided into K windows. The number of windows K corresponds to the number of observations and we also assume that each window has a corresponding state. The temporal progression of these individual windowed signal can be seen as the result of hidden states transitions. Furthermore, in each window, two sets of features using time-frequency analysis are extracted to form a feature vector. The first set of features are some common statistics, for example, mean, variance, skewness, kurtosis, entropy, Dickey-Fuller test etc. Another feature set represents signal characteristics such as peak to peak ratio, crest factor, energy, RMS, number of abrupt changes, number of small changes, mean frequency etc. We denote the feature vector of the ith window as $\boldsymbol{X^i} = (X_1^i, X_2^i, \ldots, X_L^i)^T$ where L is the number of extracted features. We normalize the elements of feature vectors $\boldsymbol{X}$ between $[-1, 1]$ to ensure they have

comparable magnitude in order to guarantee good estimation result. Figure 2 shows a windowed signal.

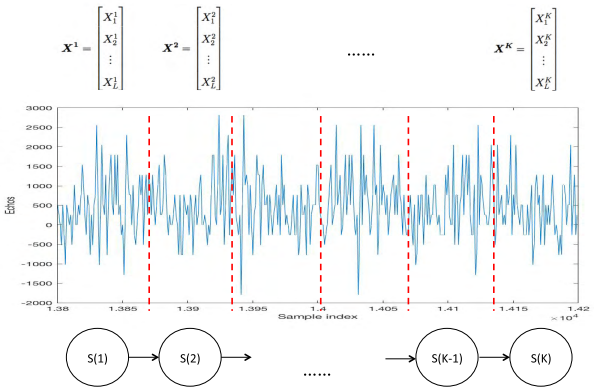

FIGURE 2. Signal is evenly divided into *K* windows and *L* features are extracted with respect in each window.

Usually, the manually picked feature set may not be an efficient presentation of the radar signals, for example, two or more features could be mutually correlated resulting possible redundancy in the feature set. The elimination of features redundancy can be done by many different criteria. In this paper, we choose to eliminate features based on their covariance matrix

$$\Sigma_{ij} = cov(X_i, X_j) = \frac{E[(X_i - \mu_{X_i})(X_j - \mu_{X_j})]}{\sigma_{X_i}\sigma_{X_j}} > \psi \qquad (19)$$

where ψ is the threshold. We select l features with less cross correlation to others. The feature relevance can also be evaluated using mutual information [19].

B. MODEL SELECTION

Hidden Markov Models provide versatile modeling structures. For applications associated with different physical processes, designing proper HMM topology is crucial for successful presentation of modeled signal. Most commonly used HMMs are ergodic and left-right (Bakis) models [20]. The ergodic model has the property that every state can be reached from other states. This means the state transition matrix $\boldsymbol{A}$ has no zero elements. The left-right model is particularly used to model signal properties change over time, for example, speech signals. The left-right model has the assumption that the states transition only occurs from lower order states to higher order states but not vice versa. To model radar target signals using HMM, the states transitions reflect radar range profiles of reflected energy and the progression of the radar echoes may contain information transferred between clutter and target locations. Therefore, an ergodic states transition model is more suitable to model radar signals.

C. HMM TRAINING AND TARGET DETECTION

After selected l features used to represent signal profile in each window, these feature vectors of different windowed signals $\boldsymbol{X} = \{\boldsymbol{X}^1, \boldsymbol{X}^2, \ldots, \boldsymbol{X}^T\}$ can be treated as distinctive observation sequences for the input of Hidden Markov Model training. To use discrete HMM, the feature vectors need to be quantized as discrete symbols using certain codebook. However, quantization may cause performance degradation due to the loss of precision. We implement continuous HMM assuming that the observation sequences are drawn from a mixture of M l-dimensional multivariate Gaussian densities. An M-component Gaussian mixture model has the form:

$$b_j(\boldsymbol{X}^t) = P(\boldsymbol{X}^t \mid S_j) \qquad (20)$$

$$= \sum_{m=1}^{M} w_{jm}\mathcal{N}(\boldsymbol{\mu}_{jm}, \boldsymbol{U}_{jm}), \qquad (21)$$

$$1 \le j \le N, 1 \le m \le M, 1 \le t \le T \qquad (22)$$

where w_{jm} is the weight parameter of the mth mixture. $\mathcal{N}$ indicates a multi-variable Gaussian density function:

$$\mathcal{N}(\boldsymbol{\mu}, \boldsymbol{U}) = \frac{1}{(2\pi)^{l/2}|\boldsymbol{U}|^{1/2}} \times \exp\left(-\frac{1}{2}(\boldsymbol{X}^t - \boldsymbol{\mu})^T\boldsymbol{U}^{-1}(\boldsymbol{X}^t - \boldsymbol{\mu})\right) \qquad (23)$$

with l mean vector $\boldsymbol{\mu}_{jm}$ and $l \times l$ covariance matrix $\boldsymbol{U}_{jm}$ for the mth mixture in state j. T denotes transpose here. The weight parameters w_{jm} have constraint:

$$\sum_{m=1}^{M} w_{jm} = 1, 1 \le j \le N, 1 \le m \le M \qquad (24)$$

Therefore, a set of parameters $\lambda = \{A, w_{jm}, \mathcal{N}(\boldsymbol{\mu}_{jm}, \boldsymbol{U}_{jm}), \pi\}$ can be used to denote a continuous HMM with Gaussian mixture observation matrix. For continuous HMM, the parameter reestimation formula is given by [3]:

$$\hat{w_{jm}} = \frac{\sum_{t=1}^{T}\gamma_t(j,m)}{\sum_{t=1}^{T}\sum_{m=1}^{M}\gamma_t(j,m)} \qquad (25)$$

$$\hat{\boldsymbol{\mu}}_{jm} = \frac{\sum_{t=1}^{T}\gamma_t(j,m)\boldsymbol{X^t}}{\sum_{t=1}^{T}\gamma_t(j,m)} \qquad (26)$$

$$\hat{\boldsymbol{U}}_{jm} = \frac{\sum_{t=1}^{T}\gamma_t(j,m)(\boldsymbol{X^t} - \boldsymbol{\mu_{jm}})(\boldsymbol{X^t} - \boldsymbol{\mu_{jm}})^T}{\sum_{t=1}^{T}\gamma_t(j,m)} \qquad (27)$$

where $\gamma_t(j,m)$ is the probability of being in state j at time t with the mth mixture component for $\boldsymbol{X}^t$:

$$\gamma_t(j,m) = \left(\frac{\alpha_t(j)\beta_t(j)}{\sum_{j=1}^{N}\alpha_t(j)\beta_t(j)}\right)\left(\frac{\omega_{jm}\mathcal{N}(\boldsymbol{\mu_{jm}}, \boldsymbol{U}_{jm})}{\sum_{m=1}^{M}\omega_{jm}\mathcal{N}(\boldsymbol{\mu_{jm}}, \boldsymbol{U}_{jm})}\right) \qquad (28)$$

IV. TRAINING DATA SET

In this work, experiments are conducted using Hidden Markov Model based target detection approach on two data sets: sense-through-foliage and sense-through-wall UWB radar data.

A. SENSE-THROUGH-FOLIAGE DATA MEASUREMENT

Sense-through-foliage data are provided by Air Force Research Lab [21]. The foliage penetration data were collected during late fall and winter with dense foliage. The principle equipments mounted on a man lift are: Barth pulser, Tektronix model 7740B oscilloscope, dual antennas and mounting stand, signal generator, rack system, custom RF switch, weather shield and power supply. The Barth pulse generator discharge a charge line using a coaxial reed switch for a very fast rise time pulse outputs. The target is a 1.5 meter trihedral metal reflector placed at 600 ft round trip distance from the base of the lift with the antenna 24 feet from the ground. Each data collection contains 16,000 samples. The total sample time duration is 0.8 μs and sample rate is approximately 20 Herz. Initially, the pulse generator was operated at low amplitude. A total of 35 reflected signals were averaged for each collection. This collection is referred as ‘‘poor" signal quality data. Later, higher amplitude transmitting pulses are applied for data collection. 100 reflected signals were averaged for each collection. This collection is referred as ‘‘good" signal quality data [22]–[24]. Previous sense-through-foliage target detection methods and foliage environment channel modeling based on the data described above can be found in [25]–[32]. In this experiment, we use the poor signal quality data set for training and testing. Moreover, data were collected from multiple radar positions with different angels toward the metal target as shown in Figure 3. Three different locations data are available for poor signal quality data. Each location includes 35 radar echoes for both target and no target cases.

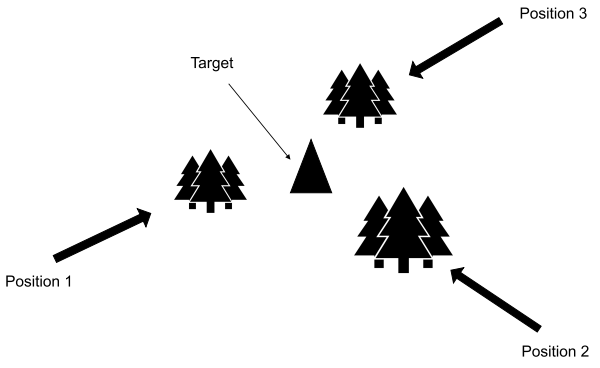

FIGURE 3. Radar echoes are collected from different positions.

B. SENSE-THROUGH-WALL DATA MEASUREMENT

Sense-through-wall data is collected using P220 UWB radar with a center frequency of 4.3GHz and 10 dB bandwidth of approximately 2.3GHz. UWB radar works in monostatic mode. A single omni-directional antenna are used to transmit pulse waveforms. The received waveforms are collected by another omni-directional antenna. The measurement were taken from different locations with different types of walls [33]–[35]. Figure 4 shows a human target standing behind a 30-cm thick gypsum wall with 6.5 feet to UWB radar on the other side. Figure 5 shows human position behind a 4-cm wooden door at a distance around 7.5 feet from UWB radar. At each location, 100 radar scans with stationary human target and no human target were collected.

V. EXPERIMENTAL RESULTS

For sense-through-foliage poor quality signal data, the target appears at around 14,000 sample with an approximate on-site duration of 250 samples. To ensure that complete target information is included, we select 400 samples around 14,000 for Hidden Markov Model training and testing. Then these 400 samples are evenly divided into different windows. Features are extracted in each window and 13 features with minimum cross-correlation to other features are selected. The covariance matrix of 13 selected features ($X1$ to $X13$) is shown at the bottom of the next page.

For 35 radar echoes at each location, we use 20 sequences for HMM training and 15 sequences for testing. Baum-Welch algorithm is used to train two HMMs for target and no target denoted as λ_{Tar} and λ_{Notar}. Figure 6 plots the Baum-Welch learning curves of 2 states and 16 states HMMs training respectively, we can observe the log-likelihood reach a plateau after several iterations which indicates the algorithm converges.

To determine appropriate number of states is important for HMM to efficiently model the signal structure. However, there's no simple theoretically correct criteria to choose the number of HMM states. Increasing the number of states usually yields higher likelihood but comes with the penalty of increasing the number of parameters which may complicate the model and lead to overfitting. There are several states discovery criteria exist in current literature [36]. A commonly used approach is to comprehensively consider Akaike Information Criteria (AIC) and Beyesian Information Criteria (BIC) for states selection:

$$AIC = -2\ln(\hat{L}) + 2p \tag{29}$$

$$BIC = -2\ln(\hat{L}) + \ln(n)p \tag{30}$$

where $\ln(\hat{L})$ is the log-likelihood, n is the number of data points and p is the number of estimated parameters. For Hidden Markov Model, the number of estimated parameters includes the elements of initial state distribution matrix π, state transition matrix A and Gaussian mixture observation matrix parameters w_{jm}, $\boldsymbol{\mu}_{jm}$ and $\boldsymbol{U}_{\boldsymbol{jm}}$.

The second terms of AIC and BIC scores are the penalty terms increasing with the number of parameters. Generally lower value of AIC/BIC indicates a good fit. For HMM, BIC usually has a larger punishment which leads to choosing more parsimonious models. Figure 7 and Figure 8 show the log-likelihood and AIC/BIC scores with increasing number of states for sense-through-foliage HMM training.

From Figure 7 we can observe that likelihood increases as number of states goes up. However, we can see prominent BIC score increasing and AIC is more steady before the

(a) (b)

FIGURE 4. Gypsum wall data measurement: (a) Location of the Human target on one side of a thick Gypsum partition wall, (b) Location of the UWB radar on the other side of a thick Gypsum partition wall.

(a) (b)

FIGURE 5. Wooden door data measurement: (a) Location of the Human target on one side of a Wooden Door, (b) Location of the UWB radar on the other side of a Wooden Door.

number of states reach to 6 as in Figure 8. The AIC/BIC scores indicate that smaller number of states may suit better for the model.

After training phase, log-likelihood of testing sequence O_{test} is calculated using both pre-trained models: $L_1 = \log P(O_{test} \mid \lambda_{Tar})$ and $L_2 = \log P(O_{test} \mid \lambda_{Notar})$,

$X1$	$X2$	$X3$	$X4$	$X5$	$X6$	$X7$	$X8$	$X9$	$X10$	$X11$	$X12$	$X13$	
0.332	0.114	0.239	0.157	−0.090	−0.006	−0.035	0.191	0.003	−0.033	0.170	0.189	−0.012	$X1$
0.114	0.324	0.234	−0.146	−0.032	−0.003	0.011	−0.028	0.020	−0.007	−0.166	−0.021	0.066	$X2$
0.239	0.234	0.312	0.006	−0.069	−0.091	−0.012	0.106	0.010	−0.042	0.004	0.110	0.035	$X3$
0.157	−0.146	0.006	0.329	−0.057	0.007	−0.111	0.201	−0.013	−0.052	0.292	0.193	−0.065	$X4$
−0.090	−0.032	−0.069	−0.057	0.300	0.026	0.044	−0.207	0.027	0.143	−0.053	−0.185	0.050	$X5$
−0.006	−0.003	−0.091	0.007	0.026	0.299	−0.007	−0.033	0.007	0.055	0.003	−0.036	−0.009	$X6$
−0.035	0.011	−0.012	−0.111	0.044	−0.007	0.304	−0.078	0.023	0.123	−0.039	−0.076	0.038	$X7$
0.191	−0.028	0.106	0.201	−0.207	−0.033	−0.078	0.322	−0.016	−0.148	0.192	0.316	−0.040	$X8$
0.003	0.020	0.010	−0.013	0.027	0.007	0.023	−0.016	0.374	0.008	−0.020	−0.011	−0.002	$X9$
−0.033	−0.007	−0.042	−0.052	0.143	0.055	0.123	−0.148	0.008	0.309	−0.007	−0.144	0.019	$X10$
0.170	−0.166	0.004	0.292	−0.053	0.003	−0.039	0.192	−0.020	−0.007	0.324	0.180	−0.062	$X11$
0.189	−0.021	0.110	0.193	−0.185	−0.036	−0.076	0.316	−0.011	−0.144	0.180	0.320	−0.038	$X12$
−0.012	0.066	0.035	−0.065	0.050	−0.009	0.038	−0.040	−0.002	0.019	−0.062	−0.038	0.339	$X13$

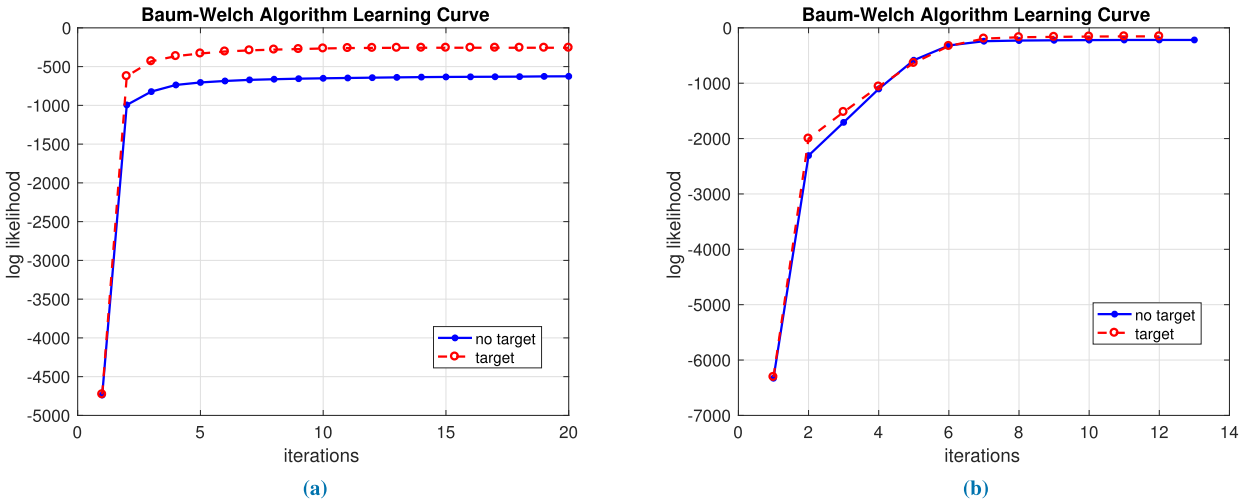

FIGURE 6. Baum-Welch training curve: (a) training with 2 states HMM, (b) training with 16 states HMM.

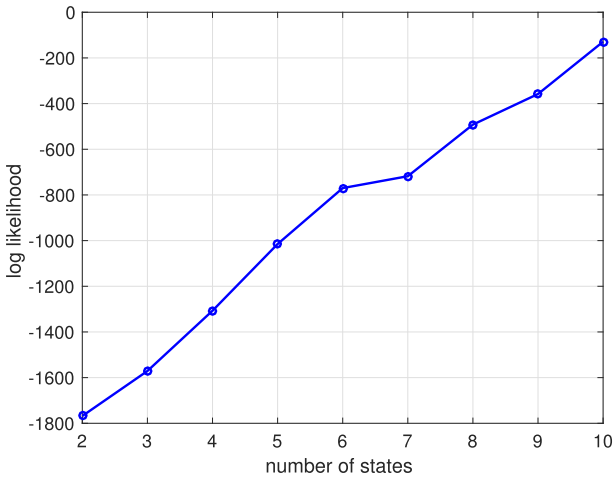

FIGURE 7. Log-likelihood increase by adding more number of states.

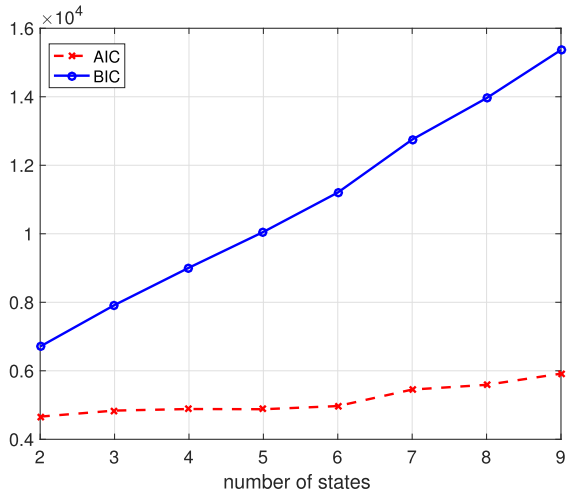

FIGURE 8. AIC/BIC scores.

the decision rule of whether the testing sequence is target or not can be formulated as a binary hypothesis testing by comparing the likelihood:

$$H_0 : \frac{L1}{L2} < \delta \quad No\ target \tag{31}$$

$$H_1 : \frac{L1}{L2} > \delta \quad Target \tag{32}$$

Where δ is a predefined threshold. The Baum-Welch algorithm requires initialization of model parameters drawn from uniform distributions which could slightly affect the training and thus the detection probability. In HMM training and testing, we use 100 Monte Carlo simulations to average out this random effect.

TABLE 1. Detection results of sense-through-foliage target with three radar positions.

Position 1		
	No target	Target
No target	99.03%	0.07%
Target	11.33%	88.67%
Position 2		
	No target	Target
No target	76%	24%
Target	17.57%	82.43%
Position 3		
	No target	Target
No target	82%	18%
Target	28%	72%

Table1 shows the confusion matrix of sense-through-foliage target detection results for three different positions (we choose $\delta = 1$ here). In Table1, position 1 gives best probability of detection of 88% with a false alarm rate of 0.07%. The other two positions data yield lower probability of detection with 82.43% and 72% and higher false alarm rate 24% and 18% respectively. Figure 9 illustrates the Receiver Operating Characteristic (ROC) curves demonstrate

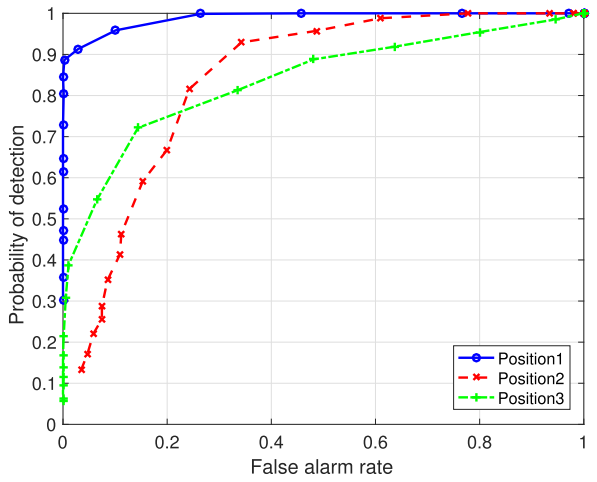

FIGURE 9. ROC curve of sense-through-foliage target detection results.

the HMM detection performance for three positions. From the ROC curve we observe that location 1 has 0.99 Area Under the Curve (AUC) while the other two locations have around 0.80 and 0.83 AUC respectively. One reason could explain the different performance among three radar locations is that trihedral reflectors consisted of three electrically conductive surfaces are used to reinforce the backscattered electromagnetic waves as the incoming waveforms from a certain direction and small variation of transmitting angels could cause low radar cross section. Considering the experiment is conducted using poor signal quality radar echoes with lower transmitting power. The testing results could be further improved if signal quality is good.

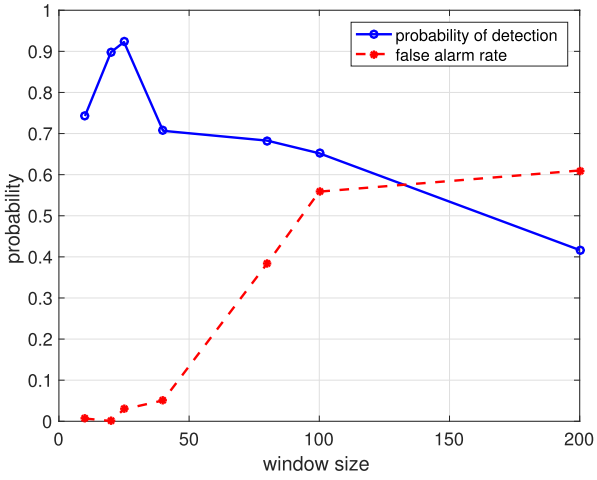

FIGURE 10. Probability of detection and false alarm rate v.s. window size.

Figure 10 shows the probability of detection and false alarm rate affected by the window size. It shows 20 samples window size gives best detection result. Intuitive explanation is that smaller window size means more observations of a given sequence are produced and they provide more reliable estimation of parameters. However, when the window size is too small (e.g. 10 samples window size shown in Figure 10), the extracted features do not have any statistical significance.

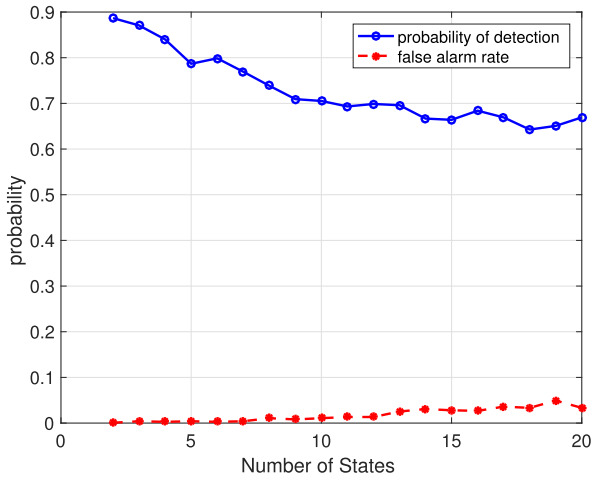

FIGURE 11. Probability of detection and false alarm rate v.s. number of states.

Figure11 shows the probability of detection and false alarm rate affected by the number of states. The result shows the probability of detection gradually decreases as the number of states increases. False alarm rate increases slowly and remains at a comparatively low level even with large number of states. The testing result also confirms that HMMs with smaller number of states have more performance gain for the UWB radar target detection task.

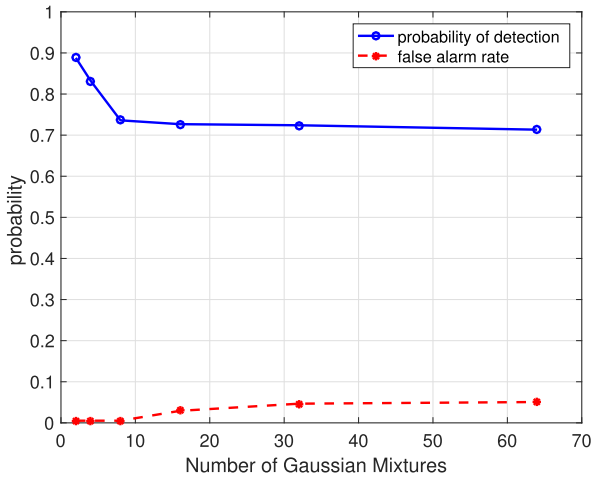

FIGURE 12. Probability of detection and false alarm rate v.s. number of Gaussian Mixtures.

Figure 12 shows the probability of detection and false alarm rate affected by the number of Gaussian Mixtures used to approximate observation probability densities. Testing results show performance degradation by using more Gaussian mixtures. However, probability of detection and false alarm rate remain stable when the number of mixtures goes large.

For sense-through-wall human target detection, we choose to use gypsum wall, wooden door and brick wall data with radar scans of no human and stationary human behind such walls. To reduce the clutter, difference between consecutive radar scans are used as HMM input:

$$\boldsymbol{Y} = \begin{bmatrix} scan(t) \\ sample1 \\ sample2 \\ \vdots \\ sampleN \end{bmatrix} - \begin{bmatrix} scan(t+1) \\ sample1 \\ sample2 \\ \vdots \\ sampleN \end{bmatrix}$$

TABLE 2. Detection results of human target behind brick wall, gypsum wall and wooden door.

Gypsum Wall		
	No human	Human
No Human	95.83%	4.17%
Human	0%	100%
Wooden Door		
	No human	Human
No Human	93.75%	6.25%
Human	5.12%	94.87%
Brick Wall		
	No human	Human
No Human	91.12%	8.88%
Human	7.14%	92.86%

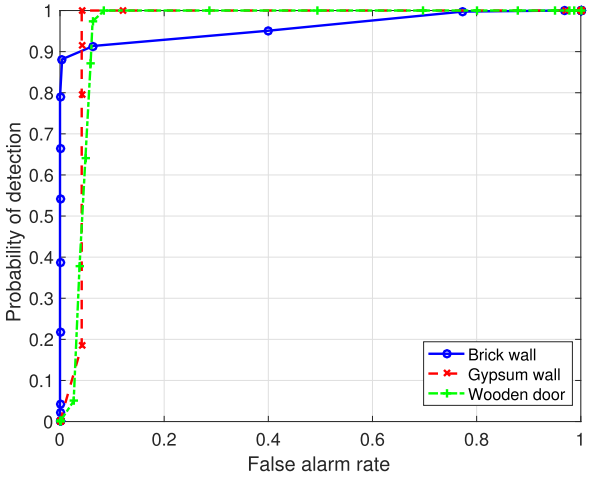

FIGURE 13. ROC curve of sense-through-wall human target detection.

In the sense-through-wall human target detection, we use $N = 2$ states, $M = 2$ Gaussian mixtures and window size $wn = 20$ samples as HMMs parameters. 2 HMMs regarding no human and stationary human are trained. Table 2 shows 100% probability of detection and 4.17% false alarm rate with human target behind gypsum wall, 94.87% probability of detection and 6.25% false alarm rate with human target behind wooden door and 92.86% probability of detection and 8.88% false alarm rate with human target behind brick wall. Further, Figure 13 illustrates the ROC curve of sense-through-wall human detection and all three curves have over 0.9 AUC which indicates robust performance.

VI. CONCLUSION

In this work, we use continuous HMMs to model UWB radar signals for target detection. UWB radar signals are windowed for feature vector extraction. Feature vector in each window serves as distinctive observation for HMMs training and testing. Sense-through-foliage and sense-through-wall experiments are conducted. Experimental results show that position 1 has best detection performance in sense-through-foliage target detection in terms of probability of detection and false alarm rate. For sense-through-wall scenario, HMMs also show good capability to distinguish between radar signals containing human target and no target. All ROC curves of sense-through-wall detection have over 0.9 AUC. HMMs parameters are also investigated and results implicate that lower number states HMMs are better for UWB radar signal modeling and target detection task.

REFERENCES

[1] J. H. Reed, *Introduction to Ultra Wideband Communication Systems* (Prentice Hall Communications Engineering and Emerging Technologies Series from Ted Rappaport). Upper Saddle River, NJ, USA: Prentice-Hall, 2005.
[2] M.-G. Di Benedetto and G. Giancola, *Understanding Ultra Wide Band Radio Fundamentals* (Prentice-Hall Communications Engineering and Emerging Technology). Englewood Cliffs, NJ, USA: Prentice-Hall, 2004.
[3] L. Rabiner, "A tutorial on hidden Markov models and selected applications in speech recognition," *Proc. IEEE*, vol. 77, no. 2, pp. 257–286, Feb. 1989.
[4] K.-F. Lee and H.-W. Hon, "Speaker-independent phone recognition using hidden Markov models," *IEEE Trans. Acoust., Speech Signal Process.*, vol. 37, no. 11, pp. 1641–1648, Nov. 1989.
[5] Y. LeCun, L. Bottou, Y. Bengio, and P. Haffner, "Gradient-based learning applied to document recognition," *Proc. IEEE*, vol. 86, no. 11, pp. 2278–2324, Nov. 1998.
[6] C. Sauper, A. Haghighi, and R. Barzilay, "Incorporating content structure into text analysis applications," in *Proc. Conf. Empirical Methods Natural Lang. Process. (EMNLP)*. Stroudsburg, PA, USA: Association for Computational Linguistics, 2010, pp. 377–387.
[7] S. Hahn *et al.*, "Comparing stochastic approaches to spoken language understanding in multiple languages," *IEEE Trans. Audio, Speech, Language Process.*, vol. 19, no. 6, pp. 1569–1583, Aug. 2011.
[8] H.-K. Lee and J. H. Kim, "An HMM-based threshold model approach for gesture recognition," *IEEE Trans. Pattern Anal. Mach. Intell.*, vol. 21, no. 10, pp. 961–973, Oct. 1999.
[9] M. Brand, N. Oliver, and A. Pentland, "Coupled hidden Markov models for complex action recognition," in *Proc. IEEE Comput. Soc. Conf. Comput. Vis. Pattern Recognit.*, San Juan, PR, USA, Jun. 1997, pp. 994–999.
[10] P. J. Moreno and R. Rifkin, "Using the Fisher kernel method for Web audio classification," in *Proc. IEEE Int. Conf. Acoust., Speech, Signal Process.*, Istanbul, Turkey, vol. 4, Jun. 2000, pp. 2417–2420.
[11] J.-L. Gauvain and C.-H. Lee, "Maximum a posteriori estimation for multivariate Gaussian mixture observations of Markov chains," *IEEE Trans. Speech Audio Process.*, vol. 2, no. 2, pp. 291–298, Apr. 1994.
[12] L. Liporace, "Maximum likelihood estimation for multivariate observations of Markov sources," *IEEE Trans. Inf. Theory*, vol. TIT-28, no. 5, pp. 729–734, Sep. 1982.
[13] B.-H. Juang, "Maximum-likelihood estimation for mixture multivariate stochastic observations of Markov chains," *AT&T Tech. J.*, vol. 64, no. 6, pp. 1235–1249, Jul./Aug. 1985.
[14] B.-H. Juang, S. Levinson, and M. Sondhi, "Maximum likelihood estimation for multivariate mixture observations of Markov chains," *IEEE Trans. Inf. Theory*, vol. TIT-32, no. 2, pp. 307–309, Mar. 1986.
[15] P. A. Devijver, "Baum's forward-backward algorithm revisited," *Pattern Recognit. Lett.*, vol. 3, no. 6, pp. 369–373, Dec. 1985.

[16] A. Viterbi, "Error bounds for convolutional codes and an asymptotically optimum decoding algorithm," *IEEE Trans. Inf. Theory*, vol. TIT-13, no. 2, pp. 260–269, Apr. 1967.
[17] L. E. Baum and T. Petrie, "Statistical inference for probabilistic functions of finite state Markov chains," *Ann. Math. Statist.*, vol. 37, no. 6, pp. 1554–1563, 1966.
[18] L. E. Baum, "An inequality and an associated maximization technique in statistical estimation of probabilistic functions of a Markov process," *Inequalities*, vol. 3, pp. 1–8, 1972.
[19] H. Peng, F. Long, and C. Ding, "Feature selection based on mutual information criteria of max-dependency, max-relevance, and min-redundancy," *IEEE Trans. Pattern Anal. Mach. Intell.*, vol. 27, no. 8, pp. 1226–1238, Aug. 2005.
[20] R. Bakis, "Continuous speech word recognition via centi-second acoustic states," in *Proc. ASA Meeting*, Washington, DC, USA, Apr. 1976.
[21] C. Dill, "Foliage penetration (Phase II) field test: Narrowband versus wideband foliage penetration," Tech. Rep. F41624-03-D-7001/04, Feb. 2006.
[22] J. Liang and Q. Liang, "Sense-through-foliage target detection using UWB radar sensor networks," *Pattern Recognit. Lett.*, vol. 31, no. 11, pp. 1412–1421, Aug. 2010.
[23] J. Liang and Q. Liang, "Outdoor propagation channel modeling in foliage environment," *IEEE Trans. Veh. Technol.*, vol. 59, no. 5, pp. 2243–2252, Jun. 2010.
[24] J. Liang, Q. Liang, and S. W. Samn, "A propagation environment modeling in foliage," *EURASIP J. Wireless Commun. Netw.*, vol. 2010, p. 873070, Dec. 2010.
[25] J. Liang, Q. Liang, and S. W. Samn, "Foliage clutter modeling using the UWB radar," in *Proc. IEEE Int. Conf. Commun.*, Beijing, China, May 2008, pp. 1937–1941.
[26] Q. Liang, S. W. Samn, and X. Cheng, "UWB radar sensor networks for sense-through-foliage target detection," in *Proc. IEEE Int. Conf. Commun.*, Beijing, China, May 2008, pp. 2228–2232.
[27] I. Maherin and Q. Liang, "Multistep information fusion for target detection using UWB radar sensor network," *IEEE Sensors J.*, vol. 15, no. 10, pp. 5927–5937, Oct. 2015.
[28] Q. Liang, X. Cheng, S. C. H. Huang, and D. Chen, "Opportunistic sensing in wireless sensor networks: Theory and applications," *IEEE Trans. Comput.*, vol. 63, no. 8, pp. 2002–2010, Aug. 2014.
[29] Q. Liang, "Situation understanding based on heterogeneous sensor networks and human-inspired favor weak fuzzy logic system," *IEEE Syst. J.*, vol. 5, no. 2, pp. 156–163, Jun. 2011.
[30] Q. Liang, "Biologically inspired target recognition in radar sensor networks," *EURASIP J. Wireless Commun. Netw.*, vol. 2010, p. 523435, Dec. 2010.
[31] Q. Liang, X. Cheng, and S. W. Samn, "NEW: Network-enabled electronic warfare for target recognition," *IEEE Trans Aerosp. Electron. Syst.*, vol. 46, no. 2, pp. 558–568, Apr. 2010.
[32] Q. Liang and X. Cheng, "KUPS: Knowledge-based ubiquitous and persistent sensor networks for threat assessment," *IEEE Trans. Aerosp. Electron. Syst.*, vol. 44, no. 3, pp. 1060–1069, Jul. 2008.
[33] S. Singh, Q. Liang, D. Chen, and L. Sheng, "Sense through wall human detection using UWB radar," *EURASIP J. Wireless Commun. Netw.*, vol. 2011, p. 20, Dec. 2011.
[34] A. Kumar, Z. Li, Q. Liang, B. Zhang, and X. Wu, "Experimental study of through-wall human detection using ultra wideband radar sensors," *Measurement*, vol. 47, pp. 869–879, Jan. 2014.
[35] X. Li, Q. Liang, and F. C. M. Lau, "Sense-through-wall human detection using the UWB radar with sparse SVD," *Phys. Commun.*, vol. 13, pp. 260–266, Dec. 2014.
[36] G. Celeux and J.-B. Durand, "Selecting hidden Markov model state number with cross-validated likelihood," *Comput. Stat.*, vol. 23, no. 4, pp. 541–564, Oct. 2008.

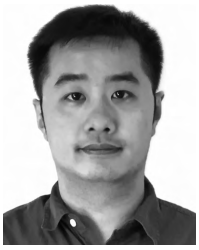

GANLIN ZHAO received the B.S. degree from Tianjin University in 2012, the M.S. degree from the University of Rochester in 2014, and the Ph.D. degree from The University of Texas at Arlington in 2017, all in electrical engineering. His research interests include wireless communications, signal processing, radar sensor networks, UWB, radar target detection, wireless sensor networks, and MIMO. He was a recipient of the Research in Motion Outstanding Graduate Scholarship Award in 2016.

QILIAN LIANG (F'01) received the Ph.D. degree in electrical engineering from the University of Southern California in 2000. Prior to joining the Faculty of The University of Texas at Arlington (UTA) in 2002, he was a Member of Technical Staff with Hughes Network Systems Inc., San Diego, CA, USA. He is currently a Distinguished University Professor with the Department of Electrical Engineering, UTA. He has authored or co-authored over 300 journal and conference papers. His research interests include wireless sensor networks, wireless communications, signal processing, and computational intelligence. He was a recipient of the 2002 IEEE Transactions on Fuzzy Systems Outstanding Paper Award, the 2003 U.S. Office of Naval Research Young Investigator Award, the 2007, 2009, and 2010 U.S. Air Force Summer Faculty Fellowship Program Award, the 2012 UTA College of Engineering Excellence in Research Award, and the 2013 UTA Outstanding Research Achievement Award, and was inducted into the UTA Academy of Distinguished Scholars in 2015.

TARIQ S. DURRANI (F'89) was a University Deputy Principal with major responsibility for University-wide strategic developments in computing/information technology infra-structure, entrepreneurship, staff development, and lifelong learning, from 2000 to 2006. He joined the University of Strathclyde, as a Lecturer in 1976, and became a Professor in 1982. He was the Department Head of one of the largest U.K. EEE Departments from 1990 to 1994. He was the Chair of the Institute for Communications and Signal Processing from 2006 to 2007, and the Head of the Centre of Excellence in Signal and Image Processing from 2008 to 2009. He has been a Vice President with Natural Sciences from 2007 to 2010, and he was an International Vice President of the Royal Society of Edinburgh–the National Academy of Scotland from 2012 to 2013. He is currently a Research Professor in electronic and electrical engineering with the University of Strathclyde. He has authored six books, and over 350 publications. He has supervised over 40 Ph.D. theses. His research interests include communications, signal processing, technology management, and higher education management. He was a Council (Board) Member, Scottish Funding Council-which distributes $3.0 billion equivalent funding annually to universities and colleges. He was the Director of the U.K. Government DTI Centre for parallel signal processing from 1989 to 1991, and the U.K. Research Council/DTI Scottish Transputer Centre, University of Strathclyde, from 1991 to 1995. He is a fellow of the Royal Academy of Engineering, the Royal Society of Edinburgh, and the IET, and is a Foreign Member of the U.S. National Academy of Engineering.